Baroclinic eddies and dust storms during autumn of MY 27.

David Hinson[1,2] and Huiqun Wang[3], [1]Carl Sagan Center, SETI Institute, Mountain View, CA 94043, USA (dhinson@seti.org), [2]Department of Electrical Engineering, Stanford University, Stanford, CA 94305, USA, and [3]Atomic and Molecular Physics Division, Smithsonian Astrophysical Observatory, Cambridge, MA 02138, USA (hwang@cfa.harvard.edu)

We are investigating martian meteorology using a combination of radio occultation data and wide-angle images obtained with Mars Global Surveyor (MGS). These two sets of observations provide a unique and accurate record of key atmospheric phenomena between about $L_s = 90°$ of Mars year 27 (MY 27) and $L_s = 120°$ of MY 28, when systematic global observations by infrared sounders are not available. (We adopt the convention that MY 1 began at $L_s = 0°$ on 11 April 1955.)

Data sets. Radio occultation experiments were conducted routinely as part of the Radio Science (RS) investigation of MGS between January 1998 and September 2006, a span of about 4.6 martian years. Each experiment yielded a profile of pressure p and temperature T versus radius and geopotential height Z that extends from the surface to the 10-Pa pressure level [1], corresponding to an altitude of about 40 km in the tropics. The uncertainties in p and T vary strongly with pressure, decreasing from about 5% at 10 Pa to about 0.3% at 610 Pa, near the surface. The uncertainty in p limits the accuracy of Z to about 30 m at 610 Pa.

The MGS Mars Orbiter Camera (MOC) systematically monitored martian aerosols and related meteorology throughout the MGS mission [e.g. 2, 3, 4, 5, 6, 7]. Mars Daily Global Maps (MDGMs) have been constructed from sets of red and blue wide-angle swaths using the method decribed by Wang and Ingersoll [3], providing essentially complete daily global coverage of the martian atmosphere with a resolution of 7.5 km per pixel.

Dynamics near the surface. As in previous work [8], we investigate eddy activity within the lowest half scale height above the surface through analysis of RS measurements of Z_{610}, the geopotential height at 610 Pa. An assortment of baroclinic eddies and stationary Rossby waves is present during autumn of the northern hemisphere at the latitudes considered here, 65°N–75°N. As an example, Fig. 1 characterizes wave activity during midautumn ($L_s = 230°$–$240°$) at 66°N. This is the spectrum of variations in Z_{610} as observed from the satellite frame at fixed local time. When viewed from this frame the frequency f of an atmospheric wave is Doppler shifted due to the rotation of Mars, so that the spectrum measures the combined effects of zonal and temporal variations. This can be expressed as

$$f = \sigma + s/\Delta\,, \qquad (1)$$

where σ is the wave frequency (cycles per sol) as observed from a fixed location on the surface, s is the zonal wave number (dimensionless), and Δ is the mean solar day (1 sol = 88,775 s). Observations of f, such as those in Fig. 1, constrain the values of σ and s but do not define them uniquely [e.g. 9, 10, 11]. With guidance from previous observations, such as Viking Lander measurements of σ [12], it is generally possible to resolve this ambiguity [8].

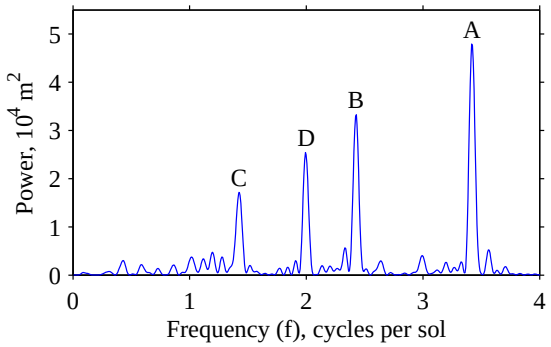

Figure 1: Power spectrum of fluctuations in Z_{610} at 66°N during $L_s = 230°$–$240°$ of MY 27. The 610-Pa pressure level is a few kilometers above the surface at the latitude and season of these measurements.

The spectrum in Fig. 1 contains 4 prominent peaks. The strongest mode, an eastward-traveling baroclinic eddy, appears at (A) $f = 3.42$ sol^{-1}, corresponding to $s = 3$, $\sigma = 0.42$ sol^{-1}. Secondary peaks associated with eddy activity appear at (B) $f = 2.42$ sol^{-1}, corresponding to $s = 2$, $\sigma = 0.42$ sol^{-1}, and (C) $f = 1.42$ sol^{-1}, corresponding to $s = 1$, $\sigma = 0.42$ sol^{-1}. These three modes have the same period, $P = 2.4$ sols, but travel eastward with different zonal phase speeds, producing an interference pattern in the form of a wave-3 disturbance whose amplitude varies significantly with longitude. This type of zonal modulation in eddy amplitude, known as a storm track, is common on Mars [e.g. 13, 14]. In addition, the spectrum in Fig. 1 includes a prominent peak at (D) $f = 2.0$ sol^{-1} that arises from a stationary wave with $s = 2$, $\sigma = 0$.

Fig. 2 shows a composite of power spectra like the one in Fig. 1, providing a compact summary of the seasonal evolution of dynamics near the surface during northern autumn of MY 27. The earliest substantial disturbance at this pressure level is a wave-1 stationary wave ($f = 1.0$ sol^{-1}) that first appears near $L_s = 160°$ and grows rapidly to a peak amplitude of about 250 m near $L_s = 170°$. Apart from a secondary peak at $L_s = 190°$, its amplitude generally decays over the next 60 sols. A wave-2 stationary wave ($f = 2.0$ sol^{-1}) appears between

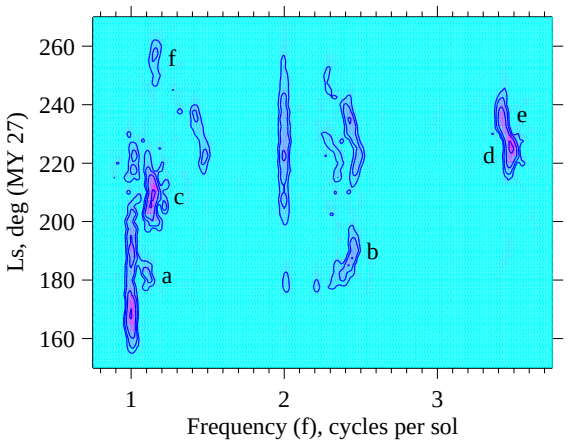

Figure 2: Evolution of baroclinic eddies and stationary waves at the 610 Pa pressure level in the northern hemisphere during autumn of MY 27. The figure is a composite of power spectra like the one in Fig. 1. Contours are shown at 0.75, 1.5, 3, and 6×10^4 m^2 s^{-2}.

$L_s = 200°$ and 260°. The amplitude of this mode peaks at about 170 m shortly after $L_s = 220°$, during a significant dust storm (see below).

As in previous years, the seasonal evolution of baroclinic eddies in autumn of MY 27 is characterized by distinctive transitions among eastward-traveling modes with different periods and zonal wave numbers [e.g. 15, 8]. Table 1 lists the properties of the six most prominent transient eddy modes, labeled a–f in Fig. 2. All results in Table 1 are derived from space-time analysis of Z_{610}. In the column headings, ϕ is latitude, s is zonal wave number, P is period, and A is amplitude. Each mode dominates for an interval of 15–20 sols, during which the other modes are weak or absent. For example, note the abrupt transition just prior to $L_s = 220°$ between mode c ($s = 1$, $P = 7.4$ sols) and mode d ($s = 3$, $P = 2.1$ sols). There is a distinct change in the period of the $s = 3$ eddies at $L_s = 230°$, from 2.1 sols for mode d to 2.4 sols for mode e. Secondary spectral peaks at $f = 1.42$ and 2.42 sol^{-1} signal the presence of storms tracks for mode e, as discussed in connection with Fig. 1; similar behavior occurs for mode d.

An important objective of this research is to compare our results with observations of eddy activity from previous years and to identify significant similarities and differences. It is immediately apparent that modes analogous to b, c, and d appeared in RS data from MY 26 [8], but there are some significant differences in amplitudes, periods, and the timing of mode transitions. Further comparisons are underway with results derived from measurements by the Viking Landers [e.g. 16, 12] and the MGS Thermal Emission Spectrometer (TES) [e.g. 14, 4, 7].

Table 1: Characteristics of prominent baroclinic eddies at 610 Pa in MY 27

Label	L_s, °	ϕ, °N	s	P, sols	A, m
a	178–186	73	1	9.4	190
b	185–195	70	2	2.2	170
c	200–215	66	1	7.4	250
d	220–230	65	3	2.1	270
e	230–240	66	3	2.4	220
f	252–262	71	1	6.5	140

The RS measurements of Z_{610} provide valuable insight into the meridional winds near the surface [8], where estimates of wind speeds are sparse. The 610 Pa pressure level is far enough above the surface to decouple the flow from surface friction (in the latitude range considered here) but far enough below the core of the intense circumpolar jet so that the flow remains near geostrophic balance. The meridional wind speed is then proportional to the zonal gradient of Z_{610}, which depends on the amplitude and zonal wave number of the baroclinic eddies.

Occultations conducted on consecutive orbits yield values of Z_{610} at fixed latitude but the measurements are not simultaneous. During the interval of 0.08 sols between each pair of observations, the measurement longitude moves westward by about 29° while the baroclinic eddies travel eastward by about 4°. The effective zonal separation of the measurements is therefore about 33°. Apart from this small correction for eddy motion, the meridional wind speed can be obtained with little difficulty, requiring no other assumptions about the period or zonal wave number of the eddies.

We applied this method of analysis to the measurements of Z_{610} that appear in Fig. 2, obtaining an estimate of the meridional wind speed for each of the 1900 cases where data are available on successive orbits. We then characterized the results through use of a distribution function. For example, Fig. 3 shows the fraction of wind speeds that exceeds 15 m s^{-1}, or F_{15}, from within a sliding 10° window of L_s. This statistic emphasizes winds in the tail of the distribution, which are particularly important because of their potential to raise dust from the surface.

The intensity of the meridional winds, as characterized in Fig. 3, varies strongly with L_s in response to variations in the amplitude and zonal wave number of the dominant eddy mode. Transitions between eddy modes with different zonal wave numbers are responsible for the most dramatic changes in F_{15}, such as a rapid increase just prior to $L_s = 220°$ in the transition from mode c ($s = 1$) to mode d ($s = 3$), followed by a rapid decrease around $L_s = 240°$ in the transition from mode e ($s = 3$) to mode f ($s = 1$). The strongest winds occur at $L_s = 220°$–230° in connection with eddy mode d,

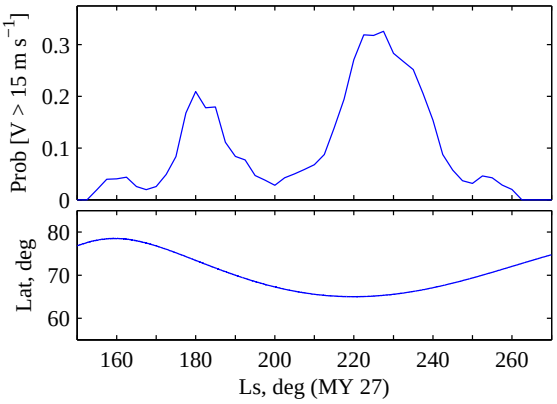

Figure 3: Seasonal variations of meridional wind speed at 610 Pa computed from RS measurements of geopotential height. (a) Fraction of wind samples whose magnitude exceeds 15 m s^{-1} from within a sliding 10° window of L_s. (b) Latitude of measurements, which drifts gradually with season.

which produces peak winds that exceed 30 m s^{-1}.

Dust storms. The MGS MOC observed a sequence of dust storms during midautumn of MY 27 [6] that was similar in some respects to what occurred at the same season in MY 24 and 26 [e.g. 2, 17, 4, 6, 7]. This sequence includes many examples of dust storms initiated by baroclinic eddies at northern midlatitudes, resulting in a dust cloud with a distinctive frontal structure. Dust activity in midautumn of MY 27 also includes several notable flushing dust storms, which begin as frontal dust storms but then travel southward through one of the major topographic basins, transporting dust into the southern hemisphere on some occasions. Wang et al. [17] have shown that a frontal dust storm can evolve into a flushing storm when eddy winds are reinforced by thermal tides, injecting dust into the return branch of the cross-equatorial Hadley circulation [see also 4, 7].

We are using MDGMs constructed from MOC wide-angle images to further characterize the frontal, flushing, and cross-equatorial dust storms of MY 27 and to investigate their relationship to the eddy activity summarized in Figs. 2 and 3. Fig. 4 shows a photogenic example of a dust storm initiated by baroclinic eddies at $L_s = 214°$–$215°$ of MY 27. MDGMs from consecutive days show the evolution of a frontal dust storm in Acidalia (upper panel) into a flushing dust storm traveling southward through the Acidalia and Chryse basins (lower panel). The leading edge of the flushing storm extends to about 20°N in the lower panel, near the landing sites of Viking Lander 1 and Pathfinder. This activity occurred during the transition between eddy modes c and d of Table 1 and Fig. 2, as the wave number of the dominant eddies was shifting from 1 to 3 and the intensity of the eddy-driven meridional winds was increasing sharply (Fig. 3).

Subsequent MDGMs reveal numerous flushing and cross-equatorial dust storms in Acidalia between $L_s = 222°$ and 226°, which became more vigorous and more regular with the onset of eddy mode d (Table 1) and its intense meridional winds (Fig. 3). The period of this mode, 2.1 sols, is conducive to the repeated occurrence of flushing dust storms [17, 4, 7]. During this same interval, dust lifting also began to occur at several locations in the southern hemisphere, including the northern rim of Hellas at $L_s = 224.5°$. The dust from these disparate sources eventually spread in longitude to encircle the planet in the southern hemisphere [6].

We plan to compile a catalog of the frontal and flushing dust storms that occurred during autumn of MY 27 and to investigate more closely their relationship with the eddy modes in Fig. 2 and Table 1. In particular, we will examine the possible influence of storm tracks on the spatial distribution of frontal and flushing dust storms.

Acknowledgments. This research is supported by NASA under Grant NNX08AL24G of the Mars Data Analysis Program.

References

[1] D. P. Hinson, R. A. Simpson, J. D. Twicken, G. L. Tyler, and F. M. Flasar. Initial results from radio occultation measurements with Mars Global Surveyor. *J. Geophys. Res.*, 104:26997–27012, 1999. doi: 10.1029/1999JE001069.

[2] B. A. Cantor, P. B. James, M. Caplinger, and M. J. Wolff. Martian dust storms: 1999 Mars Orbiter Camera observations. *J. Geophys. Res.*, 106(E10):23653–23688, 2001. doi: 10.1029/2000JE001310.

[3] H. Wang and A. P. Ingersoll. Martian clouds observed by Mars Global Surveyor Mars Orbiter Camera. *J. Geophys. Res.*, 107(E10):5078, 2002. doi: 10.1029/2001JE001815.

[4] H. Wang, R. W. Zurek, and M. I. Richardson. Relationship between frontal dust storms and transient eddy activity in the northern hemisphere of Mars as observed by Mars Global Surveyor. *J. Geophys. Res.*, 110:E07005, 2005. doi: 10.1029/2005JE002423.

[5] B. A. Cantor, K. M. Kanak, and K. S. Edgett. Mars Orbiter Camera observations of Martian dust devils and their tracks (September 1997 to January 2006) and evaluation of theoretical vortex models. *J. Geophys. Res.*, 111: E12002, 2006. doi: 10.1029/2006JE002700.

[6] B. A. Cantor. MOC observations of the 2001 Mars planet-encircling dust storm. *Icarus*, 186:60–96, 2007. doi: 10.1016/j.icarus.2006.08.019.

[7] H. Wang. Dust storms originating in the northern hemisphere during the third mapping year of Mars Global Surveyor. *Icarus*, 189:325–343, 2007. doi: 10.1016/j.icarus.2007.01.014.

[8] D. P. Hinson. Radio occultation measurements of transient eddies in the northern hemisphere of Mars. *J.*

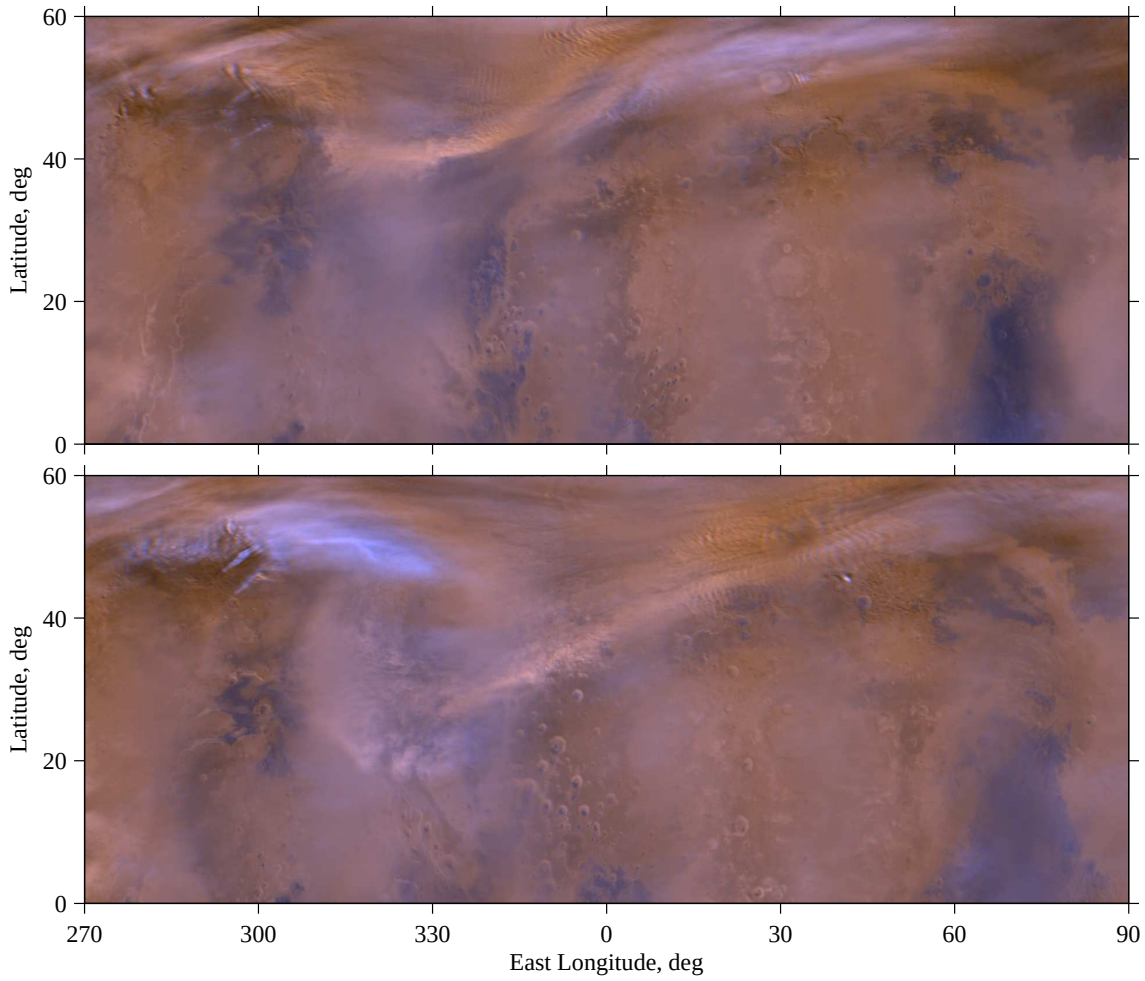

Figure 4: Dust activity on consecutive days at $L_s = 214°$–$215°$ of MY 27 as observed by the MGS MOC. Each panel shows 1/4 of a full equatorial MDGM [3]. (Top) A frontal dust storm appears in Acidalia at $45°$N, $310°$–$350°$E. (Bottom) On the following day a flushing dust storm is moving southward through the Acidalia and Chryse basins, accompanied by a nearly linear dust front extending to the northeast.

Geophys. Res., 111:E05002, 2006. doi: 10.1029/2005JE002612.

[9] W. A. Chapman, M. J. Cross, D. A. Flower, G. E. Peckham, and S. D. Smith. A spectral analysis of global atmospheric temperature fields observed by the selective chopper radiometer on the Nimbus 4 satellite during the year 1970-1. *Proc. R. Soc. London Ser. A*, 338:57–76, 1974.

[10] M. L. Salby. Sampling Theory for Asynoptic Satellite Observations. Part I: Space-Time Spectra, Resolution, and Aliasing. *J. Atmos. Sci.*, 39:2577–2600, 1982.

[11] L. R. Lait and J. L. Stanford. Applications of asynoptic space-time Fourier transform methods to scanning satellite measurements. *J. Atmos. Sci.*, 45:3784–3799, 1988.

[12] J. R. Barnes. Midlatitude disturbances in the Martian atmosphere - A second Mars year. *J. Atmos. Sci.*, 38:225–234, 1981.

[13] D. P. Hinson and R. J. Wilson. Transient eddies in the southern hemisphere of Mars. *Geophys. Res. Lett.*, 29(7): 1154, 2002. doi: 10.1029/2001GL014103.

[14] D. Banfield, B. J. Conrath, P. J. Gierasch, R. J. Wilson, and M. D. Smith. Traveling waves in the martian atmosphere from MGS TES nadir data. *Icarus*, 170:365–403, 2004. doi: 10.1016/j.icarus.2004.03.015.

[15] M. Collins, S. R. Lewis, P. L. Read, and F. Hourdin. Baroclinic Wave Transitions in the Martian Atmosphere. *Icarus*, 120:344–357, 1996. doi: 10.1006/icar.1996.0055.

[16] J. A. Ryan and R. D. Sharman. Two major dust storms, one Mars year apart - Comparison from Viking data. *J. Geophys. Res.*, 86:3247–3254, 1981.

[17] H. Wang, M. I. Richardson, R. J. Wilson, A. P. Ingersoll, A. D. Toigo, and R. W. Zurek. Cyclones, tides, and the origin of a cross-equatorial dust storm on Mars. *Geophys. Res. Lett.*, 30(9):41–1, 2003. doi: 10.1029/2002GL016828.